

Impact of Chemical Reaction on Ag-Water Nanofluid Flow and Heat Transfer Due to an Inclined Stretching Cylinder

Shikha Kandwal, Ashish Mishra, and Manoj Kumar

Department of Mathematics, Statistics and Computer Science

G. B. Pant University of Agriculture and Technology, Pantnagar, Uttarakhand, India-263145

Email: kandwal.shikha@gmail.com, ashushmishra@gmail.com, mnj_kumar2004@yahoo.com

DOI: <https://doi.org/10.29218/srmsjoms.v4i01.15908>

Abstract

Keywords: Chemical reaction; Heat transfer; Stretching Cylinder; Suction/injection; Viscous dissipation.

The object of present work is to capture the impact of chemical reaction and mass diffusion on Ag-water nanofluid along an inclined stretching cylinder. The effects of viscous dissipation and heat generation/absorption are incorporated on principal equations of the problem. The suitable transformations are used to convert governing equations into non-dimensional ODEs. Then equations with boundary conditions are solved with Runge-Kutta-Fehlberg method of 4-5th order with shooting technique. The relevant parameters impact on velocity, temperature and concentration are shown through graphs. The result shows that increasing value of chemical reaction parameter is responsible for increasing rate of mass transfer.

1. Introduction

In the terms of enhancing and decreasing the energy level related to the system, working fluids have great demands in modern thermal and manufacturing processes due to their influence on thermal conductivity and heat capacity. The ultra solid metallic suspensions in base fluid are known as nanofluid which is the main cause of the increment in thermal conductivity. This is one of the new ways for enhancing the heat transfer coefficient in the system. It has various applications in the field of biological and chemical, mechanical, civil engineering and numerous fields of applied sciences. The first investigation on nanofluid was done by Choi and Eastman [1]. They concluded that the thermal properties of base fluid can be enhanced for the better cooling after adding the nano-particles in it. After them many researchers did remarkable work on nanofluid to enhance the thermal conductivity through various geometries. Kairi and Murthy [2] worked on non-Newtonian fluid with non-Darcy porous medium to observe the influences of viscous dissipation and chemical reaction with the help of Runge-Kutta Method. Mabood et al. [3] worked on the Cu and Al₂O₃ for their MHD flow, heat transfer and mass transfer under chemical reaction and viscous dissipation on porous medium. They showed that temperature profile is an increasing function of thermophoresis parameter. Reddy et al. [4] investigated the characteristics of Ag and Cu nanoparticles with water as a base fluid over a rotating disk passing through porous media considering the chemical reaction effect. The results show the increment in concentration and temperature for both nanofluids. Zhang et al. [5] studied the radiation heat transfer of three different types of nanofluids. They considered Ag, Cu and Al₂O₃ as nanoparticles in conventional fluid. The porous medium was taken with a flat plate under chemical reaction and variable surface heat flux. Kameswaran et al. [6] worked on Cu-water as well as Ag-water under the effect of chemical reaction and viscous dissipation. Vajravelu et al. [7] considered a shrinking sheet under the viscous dissipation and radiation effects after applying the Homotopy Analysis Method. They obtained analytic solution and observed the dual solution of conducting fluid for the sheet. The research on Casson nanofluid under the effect of thermal slip and

velocity slip was done by Usman et al. [8]. Collocation method was used to solve the principal equations. Their result showed that temperature, velocity, concentration profiles are increased with the curvature parameter. Qayyum et al. [9] reported the mathematical simulation on the tangent hyperbolic nanofluid under thermal radiation, heat generation/absorption and mixed convection. Hussain et al.

[10] investigated on carbon-water nanofluid under the effect of heat generation/absorption. They considered a non-linear stretched sheet in porous space and fifth order Runge-Kutta technique was used for the mathematical solutions. Gupta et al. [11] considered an inclined stretching sheet under radiation and chemical reaction. They examined the effects of Brownian motion and thermophoresis diffusion. Dhanai et al. [12] obtained various solutions of MHD flow and behavior of heat transfer of nanofluids over a stretching/shrinking sheet under viscous dissipation. The PDEs are converted into ODEs and then solved by the finite difference method (FDM). Hsiao [13] applied thermal system for mass, heat and energy transfer on micro polar nanofluids under the viscous dissipation, Brownian motion, thermophoresis and magnetic effect to analyze their influences on nanofluid over a stretching sheet. Khan et al. [14] considered the homogeneous reaction and heterogeneous chemical reaction to examine the influence of viscous dissipation and chemical reaction on Casson liquid along with a sheet. The result shows that the concentration fields are decreased for larger value of Schmidt number. Hayat et al. [15] addressed the mixed convection flow of Casson fluid a stretching cylinder under viscous dissipation, Brownian and thermophoresis effects. The equations were converted by Homotopic procedure. There are various researchers [16-19] who have done their remarkable job in the field of fluid dynamic. References [20-24] show the recent remarkable work on nanofluid flow due to various physical effects using different numerical and analytical methods.

The aim of current research is to investigate the numerical solution of Ag-water nanofluid flow and heat transfer over inclined stretching cylinder under the influence of viscous dissipation, heat generation/absorption and suction/injection with the help of Runge-Kutta-Fehlberg method with shooting technique.

2. Mathematical Formulation

In this mathematical problem Ag-water nanofluid is considered with mixed flow in the convection form over a stretching tube along x and y axes with $z \geq 0$ (Fig. 1). The radius of given cylinder is r , K is the permeability constant, T is the temperature of nanofluid, B_0 is considered as the magnetic field strength after neglecting the induced and electric magnetic field. K_r is the chemical reaction and D_m is the mass diffusion. The more physical terminologies of nanoparticle (silver) and base fluid (water) are displayed in Table 1. The governing equations of continuity, momentum, heat and mass of nanofluid are considered as follows:

$$\frac{\partial u}{\partial x} + \frac{\partial v}{\partial y} + \frac{v}{y} = 0, \quad (1)$$

$$\rho \left(u \frac{\partial u}{\partial x} + v \frac{\partial u}{\partial y} \right) = \mu_{nf} \left(u \frac{\partial^2 u}{\partial y^2} + \frac{1}{y} \frac{\partial u}{\partial y} \right) + g(\beta\rho)_{nf}(T - T_\infty) \cos \alpha - \sigma_{nf} B_0^2 u - \frac{\mu_{nf}}{K} u, \quad (2)$$

$$(\rho c_p)_{nf} y \left(u \frac{\partial T}{\partial x} + v \frac{\partial T}{\partial y} \right) = K_{nf} \frac{\partial}{\partial y} \left(y \frac{\partial T}{\partial y} \right) - \frac{\partial}{\partial y} (y q_r) + Q_0 y (T - T_\infty) + \mu_{nf} y \left(\frac{\partial u}{\partial y} \right)^2, \quad (3)$$

$$u \frac{\partial C}{\partial x} + v \frac{\partial C}{\partial y} = D_m \frac{\partial^2 C}{\partial y^2} - K_r (C - C_\infty) \quad (4)$$

with the associated boundary conditions

$$\left. \begin{aligned} u = U_w = \frac{xU_0}{l}, v = v_w, c = c_w, T = T_w, \text{ at } y = r \\ u = 0, C \rightarrow C_\infty, T \rightarrow T_\infty, \text{ as } y \rightarrow \infty, \end{aligned} \right\} \quad (5)$$

where, $\rho_{nf} = \rho_f (1 - \phi) + \rho_{np} \phi$, is the density of nanofluid (4)

ν_{nf} and μ_{nf} are the effective kinematics viscosity and dynamic viscosity of nanofluid having a relation as:

$$\mu_{nf} = \frac{\mu_f}{(1-\phi)^{2.5}} = \nu_{nf} \rho_{nf} \quad (7)$$

$(\rho c_p)_{nf} = (\rho c_p)_f (1-\phi) + (\rho c_p)_{np} \phi$, is the heat capacitance of nanofluid. (8)

k_{nf} is the thermal conductivity and σ_{nf} is electric conductivity of nanofluid with the following expressions:

$$\frac{K_{nf}}{K_f} = \frac{K_{np} + 2K_f - 2\phi(K_f - K_{np})}{K_{np} + 2K_f + 2\phi(K_f - K_{np})} \quad (9)$$

$$\frac{\sigma_{nf}}{\sigma_f} = 1 + \frac{3\left(\frac{\sigma_{np}}{\sigma_f} - 1\right)\phi}{\left(\frac{\sigma_{np}}{\sigma_f} + 2\right) - \left(\frac{\sigma_{np}}{\sigma_f} - 1\right)\phi} \quad (10)$$

The volumetric thermal expansion coefficient is written as follows:

$$(\rho\beta)_{nf} = (\rho\beta)_f(1 - \phi) + (\rho\beta)_{np}\phi,$$

and radiative thermal heat flux q_r is given as $q_r = \frac{-16\sigma^*T^3}{3k^*} \frac{\partial T}{\partial y'}$, (11)

In the above equations ϕ represents the solid volume fraction of Ag-nanoparticles.

The subscripts nf, f, np, ∞ , and w symbolizes the properties of nanofluid, base fluid, nano-solid particles, properties at infinity and properties at surface, respectively.

Following transformations are used for present problem,

$$\xi = \frac{y^2 - r^2}{2r} \sqrt{\frac{U_0}{\nu_f l}}, u = \frac{xU_0}{l} f'(\xi), v = \frac{-r}{y} \sqrt{\frac{\nu_f U_0}{l}} f(\xi), \theta = \frac{T - T_\infty}{T_w - T_\infty}, \phi = \frac{C - C_\infty}{C_w - C_\infty} \quad (11)$$

The equation of continuity equated identically and after the transformation the mentioned equations (2)-(5) converted into:

$$(1 + 2\gamma\xi)f^m + 2\gamma f^n - M(1 - \phi)^{2.5} \frac{\sigma_{nf}}{\sigma_f} f'$$

$$-\frac{1}{\omega} f' + \lambda_1(1 - \phi)^{2.5} \left(1 - \phi + \frac{(\rho\beta)_{np}}{(\rho\beta)_f} \phi \right) \theta \cos \alpha \tag{13}$$

$$+(1 - \phi)^{2.5} \left(1 - \phi + \frac{\rho_{np}}{\rho_f} \phi \right) (-f'^2 + ff'') = 0$$

$$\frac{K_{nf}}{K_f} (2\gamma\theta'^2(1 + 2\gamma\xi)\theta'') + QPr\theta + \frac{PrEc(2\gamma\xi+1)f^{n2}}{(1-\phi)^{2.5}} + f\theta'Pr \left(1 - \phi + \frac{(\rho c_p)_{np}}{(\rho c_p)_f} \phi \right) \tag{14}$$

$$+R(\theta(\theta_w - 1) + 1)^2(3\theta'^2(1 + 2\gamma\xi)(\theta_w - 1) + 2\gamma\theta'(\theta(\theta_w - 1) + 1) + \theta^n(1 + 2\gamma\xi)(\theta(\theta_w - 1) + 1)) = 0,$$

$$(2\gamma\xi + 1)\phi^n + (fSc + \lambda)\phi' - ScC_r\phi = 0 \tag{15}$$

$$\left. \begin{aligned} f(0) = S, f'(0) = 1, \theta(0) = 1 \\ f(\infty) = S, \theta(\infty) = 0, \phi(0) = 1 \\ \phi(\infty) = 0. \end{aligned} \right\} \tag{16}$$

The present problem has non-dimensional parameters as:

$\omega = \frac{KU_0}{v_f l}$ where, ω represents porosity parameter, $Q = \frac{Q_0 l}{U_0(\rho c_p)_f}$ is heat generation/ absorption, $Ec = \frac{U_0^2 x^2}{l^2(\rho c_p)_f(T_w - T_\infty)}$ is Eckert number, $\gamma = \sqrt{\frac{lv_f}{U_0 r^2}}$ is a curvature parameter, $Pr = \frac{(\rho c_p)_f v_f}{k_f}$ where Pr is Pradtl number, $M = \frac{\sigma_f B_0^2 l}{\rho_f U_0}$ is the Hartmann number $S = -v_w \sqrt{\frac{1}{v_f U_0}}$ is suction/injection, $\lambda_1 = \frac{Gr_x}{Re_x^2} = \frac{g\beta_f l^2}{U_0^2 x}$ ($T_w - T_\infty$) is mixed convection parameter, $R = \frac{16\sigma^* T_\infty^3}{3\sigma^* k_f}$ is radiation parameter, $\theta_w = \frac{T_w}{T_\infty}$ is temperature ratio parameter, $Sc = \frac{v_f}{D_m}$ denotes the Schmidt number, $C_r = \frac{k_r}{(U_0/l)}$ where C_r is chemical reaction.

The physical quantities C_{fx} and Nu_x are:

$$C_f = \frac{\tau_{rw}}{\rho_f U_w^2} \text{ is the skin fraction coefficient} \tag{17}$$

$$Nu_x = \frac{xq_w}{k_f(T_w - T_\infty)} \text{ is the Nusselt number} \tag{18}$$

$$Sh_x = \frac{xq_w}{(C_w - C_\infty)} \text{ is the Sherwood number} \tag{19}$$

where τ_r and q_w are given as:

$$\tau_w = \mu_{nf} \left(\frac{\partial u}{\partial r} \right) \Big|_{y=r} \text{ is shear stress and } q_w = -k_{nf} \left(\frac{\partial T}{\partial r} \right) \Big|_{y=r} + (q_r)_w \text{ is wall heat flux.} \tag{20}$$

The skin friction and Nusselt number in non-dimensional form are as follows:

$$C_f = \frac{f''(0)}{(1-\phi)^{2.5} Re_x^{0.5}}, \quad (21)$$

$$Nu_x = \left(\frac{k_{nf}}{k_f} + R\theta_w^3 \right) \theta'(0) Re_x^{0.5} \quad (22)$$

where $Re_x = \frac{U_w x}{\nu_f}$ is local Reynolds number.

3. Numerical Method

The non-dimensional momentum equation (13), energy equation (14) and concentration equation (15) with boundary condition (16) are solved mathematically by the help of RKF method of fourth-fifth order with a shooting algorithm by considering $y_1 = f, y_2 = f', y_3 = f'', y_4 = \theta, y_5 = \theta', y_6 = \phi, y_7 = \phi'$. The obtained set of first order ODEs are achieved as follows:

$$\begin{aligned} y_1' &= y_2 \\ y_2' &= y_3 \\ y_3' &= \frac{\left(MA_1 A_4 y_2 + \frac{y_2}{\omega} - \lambda A_1 A_3 y_4 \cos \alpha + y_2 y_2 A_1 A_2 - y_1 y_3 A_1 A_2 - 2\gamma y_3 \right)}{(1 + 2\gamma\xi)} \\ y_4' &= y_5 \\ y_5' &= \frac{\left(-2\gamma y_5 A_5 - R(y_4(\theta_w - 1) + 1)^2 \left(\frac{3y_5^2(1 + 2\gamma t)(\theta_w - 1)}{-2\gamma y_5(y_4(\theta_w - 1) + 1)} \right) \right.}{\left. -y_1 y_5 A_6 Pr - QPr y_4 - \frac{EcPr(1 + 2\gamma\xi)y_3^2}{A_1} \right)}{(A_5(1 + 2\gamma\xi) + (1 + 2\gamma\xi)(y_4(\theta_w - 1) + 1)^3 R)} \\ y_6' &= y_7 \\ y_7' &= \frac{y_6 Cr Sc - (y_1 Sc + \lambda)y_7}{(1 + 2\gamma\xi)} \end{aligned} \quad (23)$$

where, $A_1 = (1 - \phi)^{2.5}, A_2 = 1 - \phi + \frac{\rho_s}{\rho_f} \phi, A_3 = 1 - \phi + \frac{(\rho\beta)_s}{(\rho\beta)_f} \phi, A_4 = \frac{\sigma_{nf}}{\sigma_f} \phi, A_5 = 1 - \phi + \frac{(\rho c_p)_s}{(\rho c_p)_f} \phi$, are

constants, and consequent initial conditions are:

$$\begin{pmatrix} y_1 \\ y_2 \\ y_3 \\ y_4 \\ y_5 \\ y_6 \\ y_7 \end{pmatrix} = \begin{pmatrix} S \\ 1 \\ p_1 \\ 1 \\ p_2 \\ 1 \\ p_3 \end{pmatrix}$$

The system of first order ODEs (23) together and preliminary conditions (24) are solved with using a 4-5th order RKF integration procedure and appropriate values of unknown conditions p_1, p_2 and p_3 are determined for a number of appropriate values of S . The evaluated values of $f'(\xi)$, $\theta(\xi)$ and $\phi(\xi)$ as $\xi=0$, during specified boundary conditions $f'(\infty) = 0$, $\theta(\infty) = 0$ and $\phi(\infty) = 0$ get contrast. To achieve an better evaluation for the solution, we regulate the approximated values of p_1, p_2 and p_3 . The unknown constant parameters p_1, p_2 and p_3 are approximated by Newton's scheme in such a way that boundary conditions at large numerical values of $\xi \rightarrow \infty$ have error below 10^{-6} .

4. Code Validation

The results are bonafide by comparing our results with Butt et al. [16] and Ishak and Nazar [18] for a flat surface shown in Table 2. The value of Nusselt number for different values of Prandtl number are compared with our results and the use of present code is justified because the results establish a decent agreement.

5. Results and Discussion

We used non-linear ordinary differential equations (ODEs) and partial differential equations (PDEs) to solve the problem and deal with the outcomes of mathematical calculation which converted from non-linear PDEs into ODEs. The attained governing equations have been figured out and solved by the Runge-Kutta-Fehlberg method considering the boundary conditions with shooting method. The results of non-dimensional terms such as temperature profile, Schmidt number and Prandtl number are discussed. The value of mesh size are taken $\Delta\xi = 0.001$, where ξ is the domain of similarities variable. Also, $1 \leq \xi \leq 8$, $\phi = 0.1$ and $R = 0.7$ are considered fixed during the whole calculations. Here, we have considered the colloidal suspensions Ag-nanoparticles into water. In the absence of Ag-nanoparticles i.e. for pure water, the value of solid volume fraction ($\phi = 0$) is always taken as zero. The results have been shown graphically, also the computational values of $(-f''(0))$ and $(-\theta'(0))$ and $(-\phi'(0))$ for Ag-water have been displayed in Table 2 and observed the variation in Schmitt number, chemical reaction and Prandtl number with respect to different physical profiles such as velocity, temperature and concentration. On observing Figure 2, we observed that concentration profile is decreasing on increasing the value of the Schmitt number (Sc). The same trend has been shown by Figure 3, where concentration profile of Ag-nanoparticles is decreasing with the acceleration of chemical reaction parameter. Table 3 suggests that the absolute value of skin friction $f''(0)$ and Nusselt number $-\theta'(0)$ remain same but the value of increases with Cr . The next three figures, i.e. Figures 4 to 6 represent the change in velocity, temperature and concentration profiles due to the Prandtl number with the fixed parameters. In case of increasing Prandtl number (Pr) at $M = 1.0$, $R = 0.7$, $\theta_w = 1.1$, $\gamma = 0.2$, $Sc = 1.0$ and $Cr = 0.1$, the velocity profile attained maximum value for lower values of Pr . Figure 4

shows that the temperature decreases on escalating the value of Pr but the opposite effect is observed on concentration profile which means increasing value of Prandtl number hikes the concentration profile of Ag-nanoparticles. Also, it is observed from Table 3, both skin friction and Nusselt number are increased but the reverse trend has been found in Sherwood number. Figure 7 reflects the influence on skin friction coefficient due to the Eckert number and heat generation/absorption Q for Ag-water nanofluid. It shows that the skin friction coefficient is increased with the increasing values of Eckert number and heat generation/absorption. The variations due to the Eckert number and heat generation/absorption on Nusselt number and Sherwood number are explained in Figures 8 and 9, respectively. It is observed from figure that the Nusselt number decreases for escalating values of Ec and Q while Sherwood number shows the contrary effects in Figure 8 on comparing with Figure 7. Table 4 reveals that the absolute value of skin friction and Nusselt number depreciated for each value of Eckert number when heat generation (or absorption) parameter Q , accelerates; whereas, the opposite behavior found for Sherwood number.

Moreover, Figs. 10, 11 and 12 represent the variation in C_f , Nu_x , and Sh_x , with respect to Hartmann number M and ϕ solid volume fraction, when $Pr = 6.2, Sc = 1.0, \lambda = 1.6, R = 0.7$ and $Q = 0.1$ are fixed. Figure 10 shows the variation in skin friction coefficient which decreases due to Hartmann number as well as solid volume fraction. Similarly, Figures 11 and 12 demonstrates the reduction in Nusselt number and Sherwood number with the increasing value of M and ϕ . On analyzing table 5 we establish that the dimensionless term skin friction coefficient accelerates on enhancing the value of M , for the particular numerical value of nanoparticles volume fraction, while Nusselt and Sherwood numbers are decreased on enhancing the value of M with ϕ .

Table 1: Thermo-physical properties of pure water and Ag-nanoparticle.

	$\kappa(\text{W/mK})$	$\rho(\text{Kg/m}^3)$	$\sigma(\text{Um})^{-1}$	$c_p(\text{J/KgK})$	$\beta \times 10^{-5}(1/K)$
Silver (Ag)	429	10490	6.30×10^7	235	1.89
Water (H ₂ O)	0.613	997.1	0.05	4179	21

Table 2: Comparison of numerical values of $(-\theta'(0))$ when, $\gamma = M = \omega = \lambda_1 = 0, R = \phi = 0$.

Pr	$(-\theta'(0))$		
	Ishak and Nazar [18]	Butt et al. [16]	Present study
1.0	0.5820	0.5820	0.5818299
10.0	2.3080	2.3080	2.3079730

Table 3: Several values of $f''(0)$, $\theta'(0)$ and $\phi'(0)$, when $M = 1.0$, $R = 0.7$, $\gamma = 0.2$, $\lambda = 1.6$ $\theta_w = 1.1$.

Sc	Cr	Pr	$-f''(0)$	$-\theta'(0)$	$-\phi'(0)$
0.2			1.763416	1.298530	0.298744
0.4			1.763416	1.298530	0.416434
0.6			1.763416	1.298530	0.539934
0.8			1.763416	1.298530	0.666134
1.0			1.763416	1.298530	0.792734
1.0	0.1		1.763416	1.298530	0.792734
	0.3		1.763416	1.298530	0.958284
	0.5		1.763416	1.298530	1.089965
	0.7		1.763416	1.298530	1.202449
	0.9		1.763416	1.298530	1.302305
	0.1	1	1.446736	0.264447	0.871850
		2	1.534395	0.449825	0.847000
		3	1.609136	0.652711	0.827150
		4	1.669667	0.858601	0.812360
		5	1.717995	1.061601	0.801660
		6	1.756650	1.259601	0.793999

Table 4: Influence on skin friction, Nusselt number and solid volume fraction due to Ec and Q when $Pr = 6.2$, $R = 0.7$, $\lambda = 1.6$, $Cr=0.1$ and $Sc=1$

Q	skin friction coefficient			Nusselt number			Sherwood number		
	Ec			Ec			Ec		
	0.1	0.3	0.5	0.1	0.3	0.5	0.1	0.3	0.5
-0.2	-3.63853331	-3.60993609	-3.58197476	3.78145833	2.70471068	1.65800373	0.773055	0.775395	0.777665
-0.1	-3.617563182	-3.587545716	-3.558275936	3.428620577	2.342236468	1.288193107	0.775585	0.778105	0.780565
0	-3.59077229	-3.55913018	-3.52836154	3.019370459	1.924062856	0.863781839	0.778994	0.781735	0.784375
0.1	-3.55402915	-3.52051434	-3.48810009	2.51721313	1.41536185	0.35209223	0.783905	0.786905	0.789775
0.2	-3.497569311	-3.462463917	-3.428612817	1.835431824	0.737570234	-0.31883341	0.791805	0.795005	0.798075

Table 5: Influence on skin friction, Nusselt number and solid volume fraction due to ϕ and M when $Pr = 6.2$, $R = 0.7$, $\lambda = 1.6$, $Cr=0.1$ and $Sc = 1$

M	Skin friction coefficient			Nusselt number			Sherwood number		
	ϕ			ϕ			ϕ		
	0.01	0.02	0.03	0.01	0.02	0.03	0.01	0.02	0.03
0.7	-1.603286857	-1.684779619	-1.76717498	2.855518865	2.833652814	2.812671232	0.80702	0.80448	0.80221
1.0	-1.699765975	-1.783070701	-1.86742005	2.797625804	2.775245738	2.753792205	0.799095	0.796735	0.79462
1.6	-1.879531257	-1.966431689	-2.05454525	2.689779332	2.666306901	2.643476638	0.78533	0.78326	0.78141

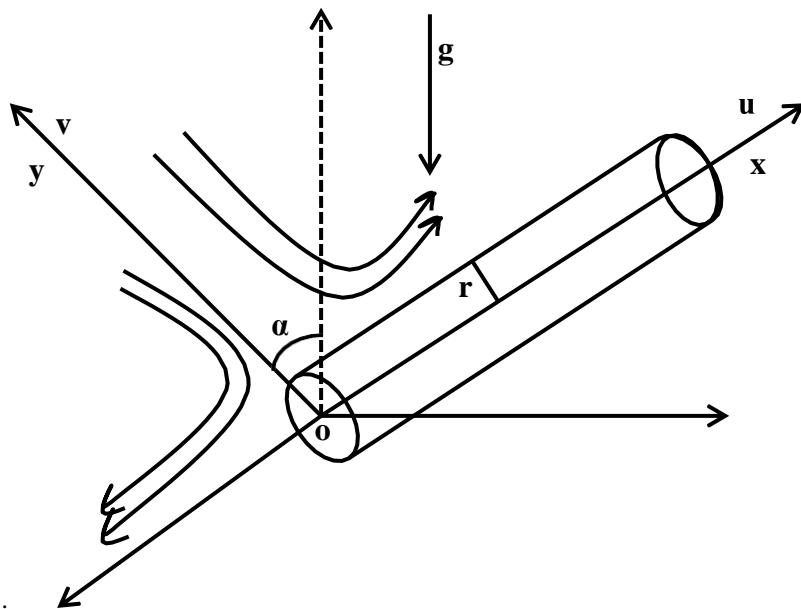


Fig. 1: Flow geometry

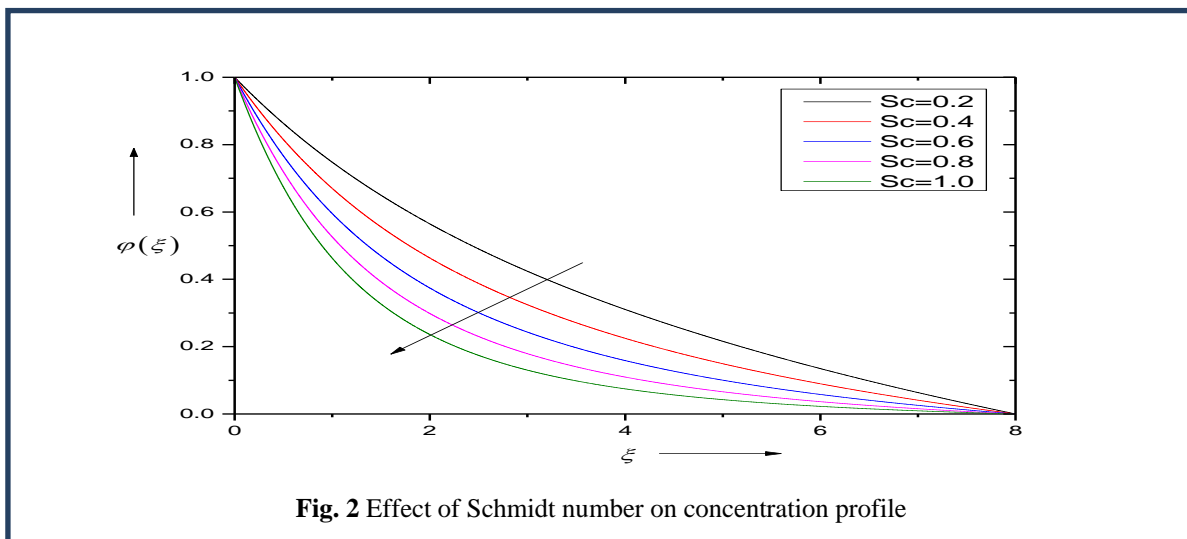
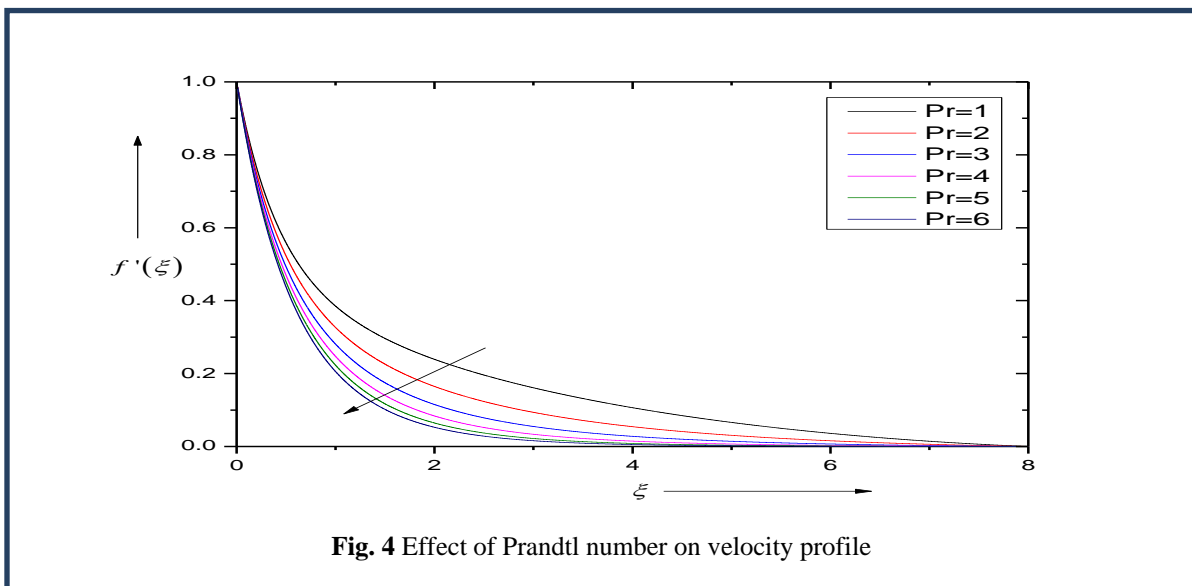
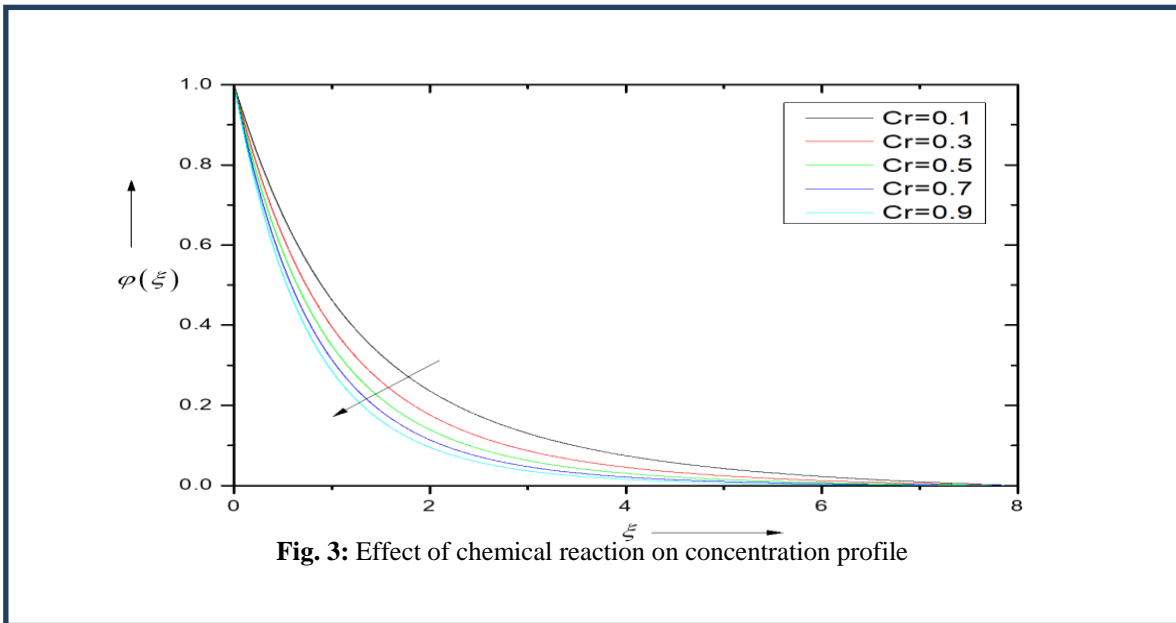
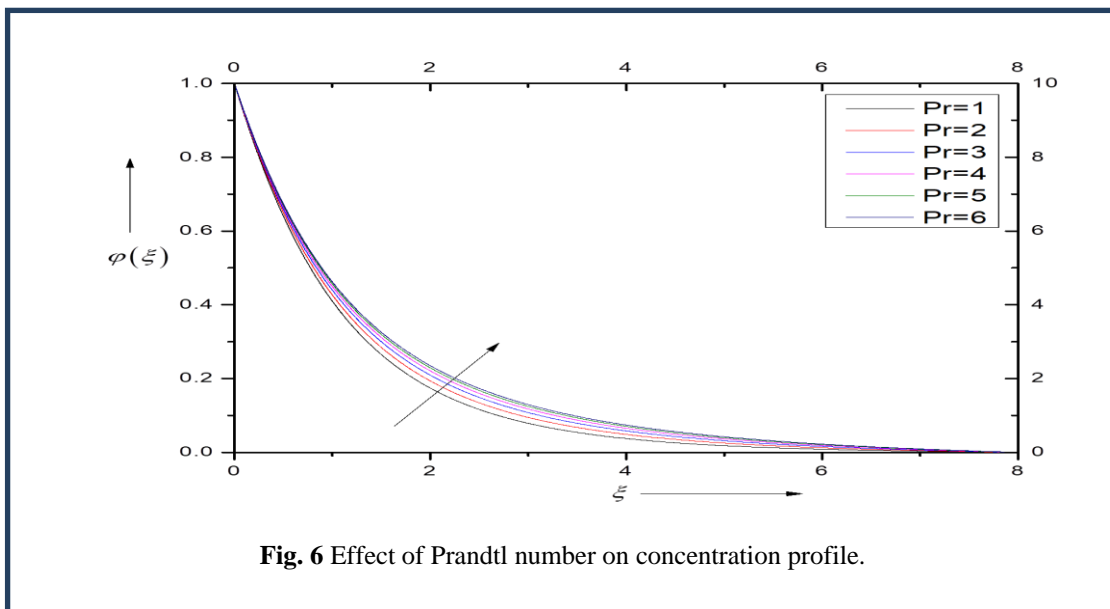
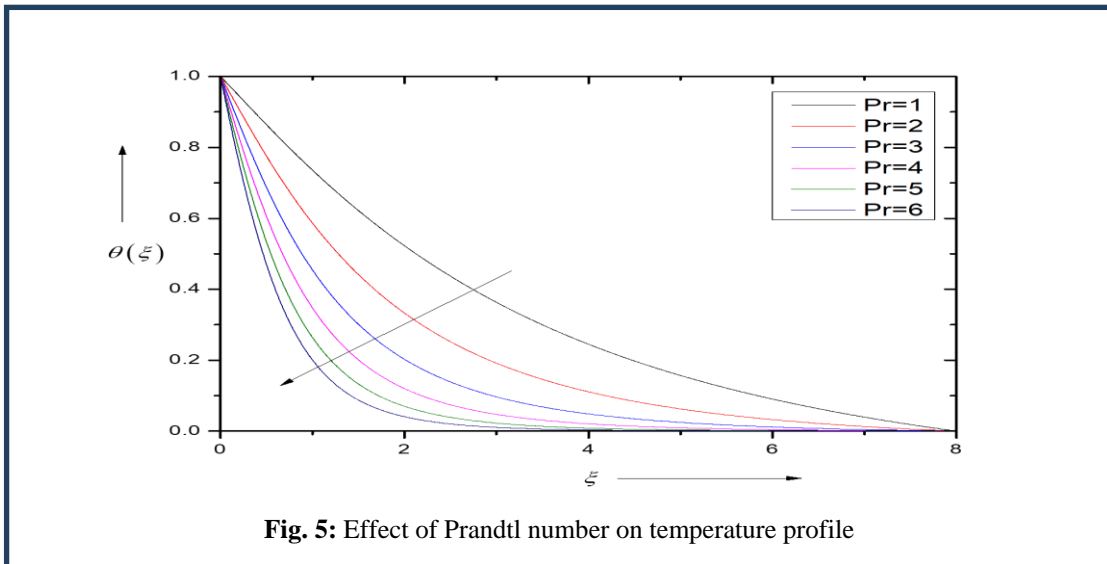
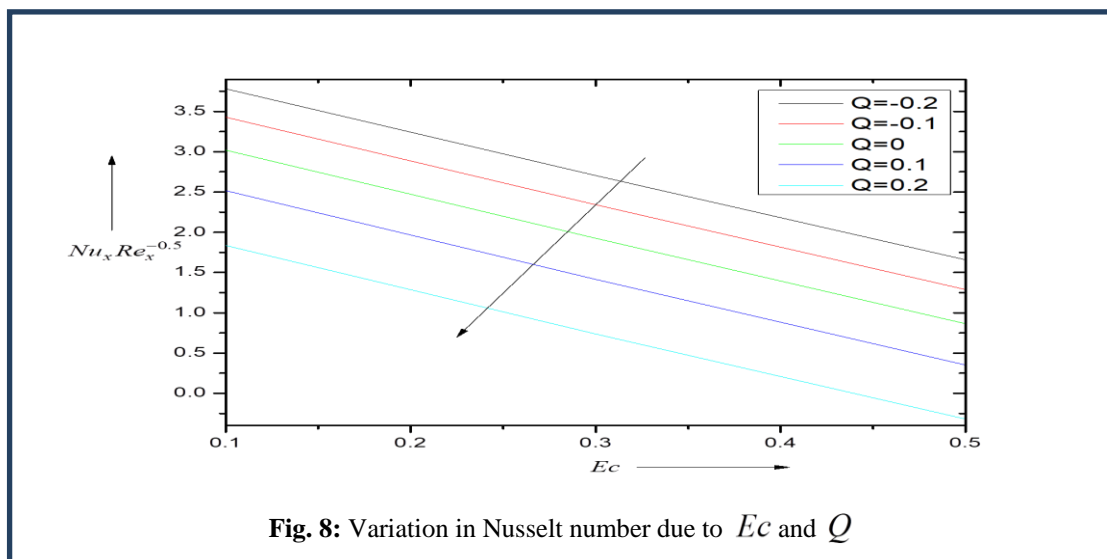
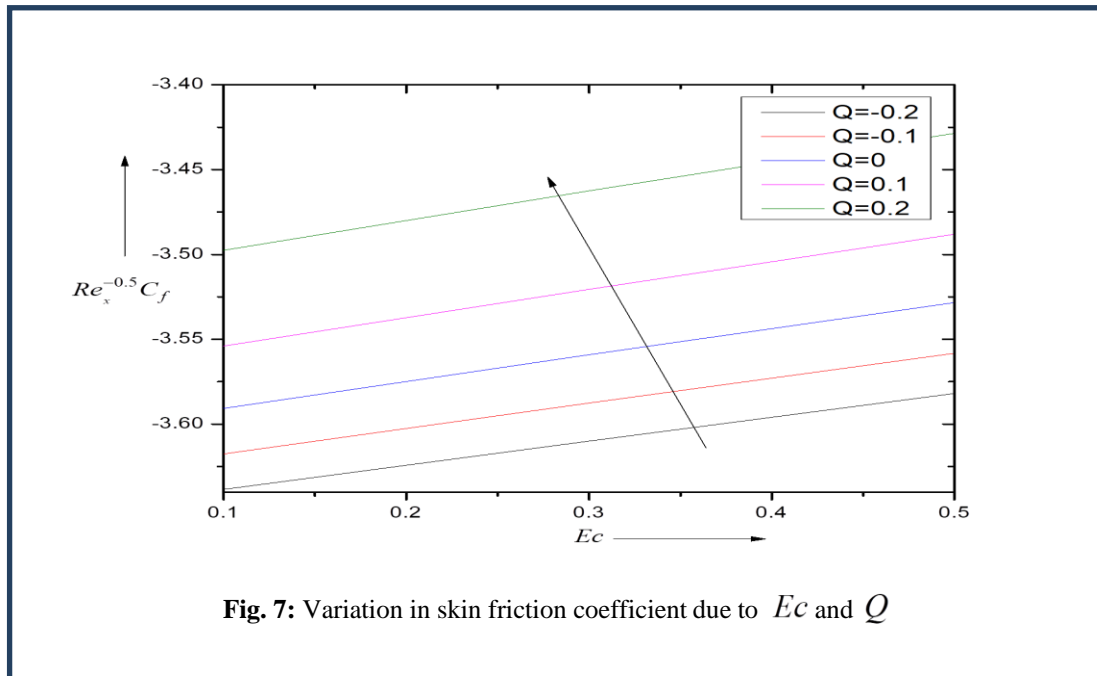
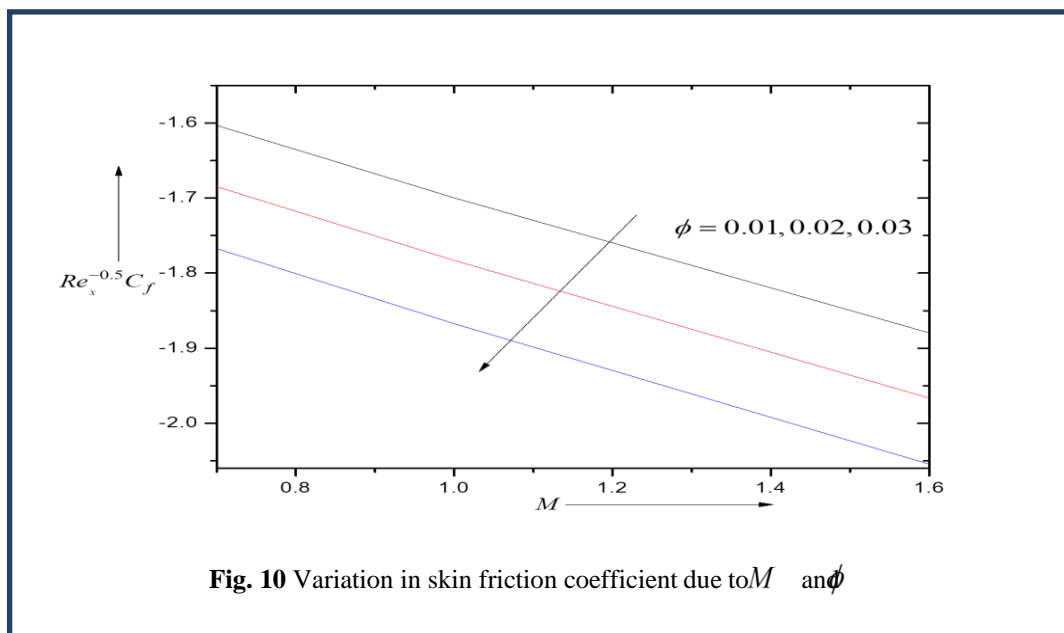
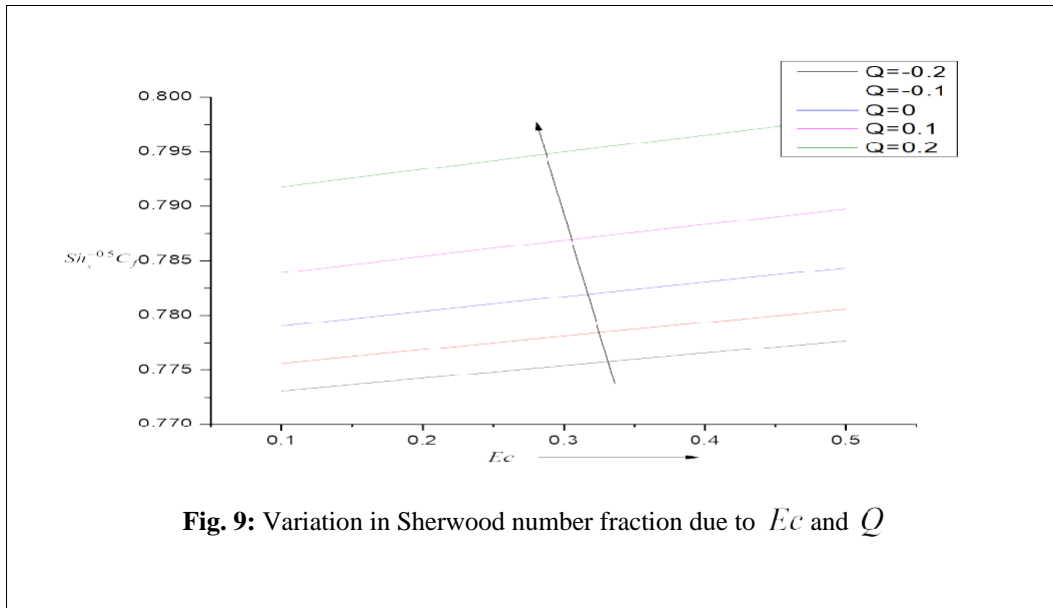


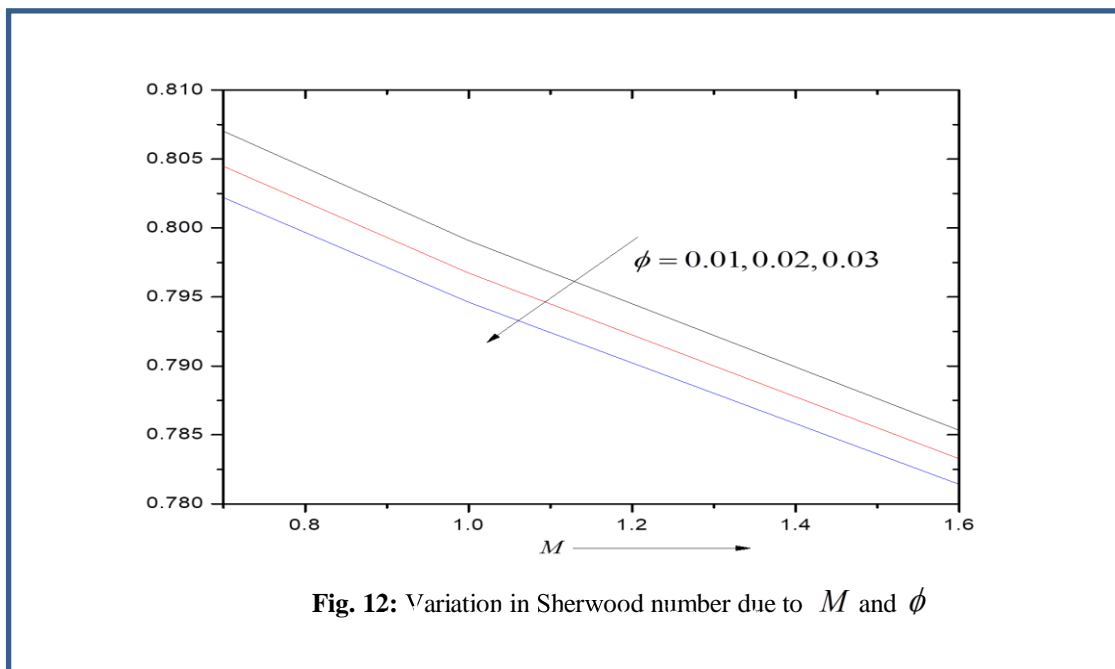
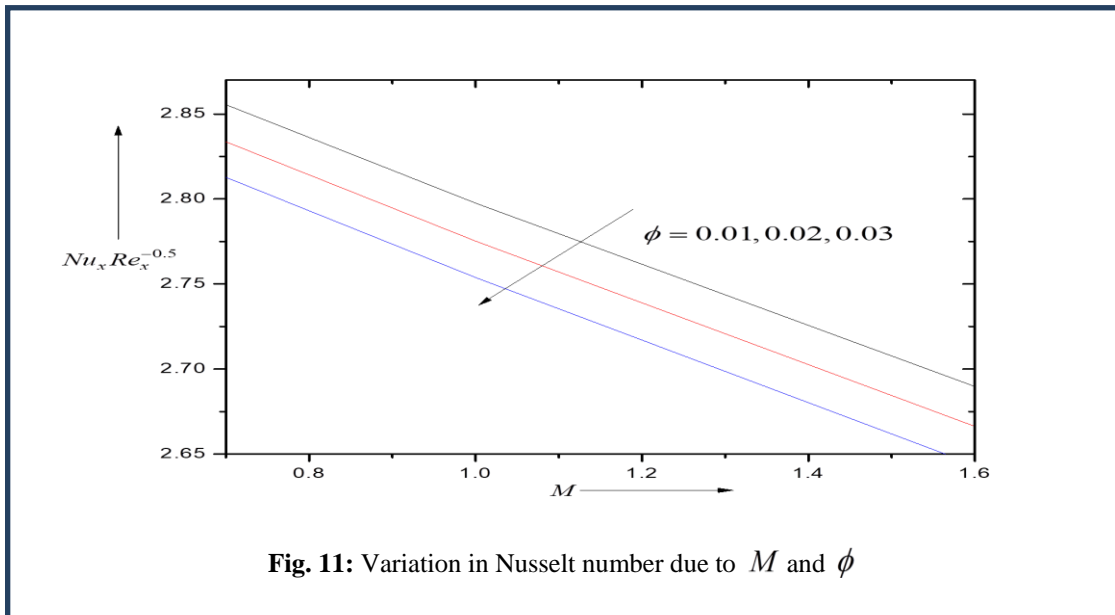
Fig. 2 Effect of Schmidt number on concentration profile











6. Conclusion

Some important outcomes of the current analysis define as follows:

- There is no change made by Schmidt number and chemical reaction for both (velocity and temperature) profiles, whereas the concentration profile decreases with Schmidt number and chemical reaction.
- With the increment in Prandtl number, velocity and temperature profile shows reduction but concentration profile shows increment.
- The skin friction coefficient and Sherwood number get increased with increasing value of Eckert number Ec and heat generation/absorption Q and they are decreased with Hartmann number M and solid volume fraction parameter ϕ .
- The Nusselt number is decreased in both the cases, i.e. with Eckert number and heat generation/absorption, and also with Hartmann number and solid volume fraction.

References

- [1] S.U.S. Choi & J.A. Eastman. Enhancing thermal conductivity of fluids with nanoparticles. United States, 1995.
- [2] Kairi, R. R., & Murthy, P. V. S. N. Effect of viscous dissipation on natural convection heat and mass transfer from vertical cone in a non-Newtonian fluid saturated non-Darcy porous medium. *Applied Mathematics and Computation*. 217(20): 8100-8114, 2011.
- [3] Mabood, F., Shateyi, S., Rashidi, M. M., Momoniat, E., & Freidoonimehr, N. MHD stagnation point flow heat and mass transfer of nanofluids in porous medium with radiation, viscous dissipation and chemical reaction. *Advanced Powder Technology*. 27(2): 742-749, 2016.
- [4] Reddy, P. S., Sreedevi, P., & Chamkha, A. J. MHD boundary layer flow, heat and mass transfer analysis over a rotating disk through porous medium saturated by Cu-water and Ag-water nanofluid with chemical reaction. *Powder technology* 307: 46-55, 2017.
- [5] Zhang, C., Zheng, L., Zhang, X., & Chen, G. MHD flow and radiation heat transfer of nanofluids in porous media with variable surface heat flux and chemical reaction. *Applied Mathematical Modelling*. 39(1): 165-181, 2015.
- [6] Kameswaran, P. K., Narayana, M., Sibanda, P., & Murthy, P. V. S. N. Hydromagnetic nanofluid flow due to a stretching or shrinking sheet with viscous dissipation and chemical reaction effects. *International Journal of Heat and Mass Transfer*. 55(25-26): 7587-7595, 2012.
- [7] Vajravelu, K., Sarojamma, G., Sreelakshmi, K., & Kalyani, C. Dual solutions of an unsteady flow, heat and mass transfer of an electrically conducting fluid over a shrinking sheet in the presence of radiation and viscous dissipation. *International Journal of Mechanical Sciences*. 130: 119-132, 2017.
- [8] Usman, M., Soomro, F. A., Haq, R. U., Wang, W., & Defterli, O. Thermal and velocity slip effects on Casson nanofluid flow over an inclined permeable stretching cylinder via collocation method. *International Journal of Heat and Mass Transfer*. 122: 1255-1263, 2018.
- [9] Qayyum, S., Hayat, T., Shehzad, S. A., & Alsaedi, A. Mixed convection and heat generation/absorption aspects in MHD flow of tangent-hyperbolic nanofluid with Newtonian heat/mass transfer. *Radiation Physics and Chemistry*. 144: 396-404, 2018.
- [10] Hussain, Z., Hayat, T., Alsaedi, A., & Ahmad, B. Three-dimensional convective flow of CNTs nanofluids with heat generation/absorption effect: A numerical study. *Computer Methods in Applied Mechanics and Engineering*. 329: 40-54, 2018.
- [11] Gupta, S., Kumar, D., & Singh, J. MHD mixed convective stagnation point flow and heat transfer of an incompressible nanofluid over an inclined stretching sheet with chemical reaction and radiation. *International Journal of Heat and Mass Transfer*. 118: 378-387, 2018.

- [12] Dhanai, R., Rana, P., & Kumar, L. Multiple solutions of MHD boundary layer flow and heat transfer behavior of nanofluids induced by a power-law stretching/shrinking permeable sheet with viscous dissipation. *Powder Technology*. 273: 62-70, 2015.
- [13] Hsiao, K. L. Micropolar nanofluid flow with MHD and viscous dissipation effects towards a stretching sheet with multimedia feature. *International Journal of Heat and Mass Transfer*. 112: 983-990, 2017.
- [14] Khan, M. I., Hayat, T., Khan, M. I., & Alsaedi, A. A modified homogeneous-heterogeneous reactions for MHD stagnation flow with viscous dissipation and Joule heating. *International Journal of Heat and Mass Transfer*. 113: 310-317, 2017.
- [15] Hayat, T., Khan, M. I., Waqas, M., Yasmeen, T., & Alsaedi, A. Viscous dissipation effect in flow of magnetonanofluid with variable properties. *Journal of Molecular Liquids*. 222: 47-54, 2016.
- [16] Butt, A. S., Ali, A., & Mehmood, A. Numerical investigation of magnetic field effects on entropy generation in viscous flow over a stretching cylinder embedded in a porous medium. *Energy*. 99: 237-249, 2016.
- [17] Hayat, T., Ahmad, S., Khan, M. I., & Alsaedi, A. Modeling and analyzing flow of third grade nanofluid due to rotating stretchable disk with chemical reaction and heat source. *Physica B: Condensed Matter*. 537: 116-126, 2018.
- [18] Ishak, A. M., & Nazar, R. M. Laminar boundary layer flow along a stretching cylinder. *European Journal of Scientific Research*. 36(1): 22-29, 2009.
- [19] Khan, M., Shahid, A., Malik, M. Y., & Salahuddin, T. Thermal and concentration diffusion in Jeffery nanofluid flow over an inclined stretching sheet: A generalized Fourier's and Fick's perspective. *Journal of Molecular Liquids*. 251: 7-14, 2018.
- [20] Mishra, A., & Kumar, M. Influence of viscous dissipation and heat generation/absorption on Ag-water nanofluid flow over a Riga plate with suction. *International Journal of Fluid Mechanics Research*. 46(2): 113- 125, 2019.
- [21] Mishra, A., & Kumar, M. Viscous dissipation and joule heating influences past a stretching sheet in a porous medium with thermal radiation saturated by silver–water and copper–water nanofluids. *Special Topics & Reviews in Porous Media: An International Journal*, 10(2): 171-186, 2019.
- [22] Dogonchi, A. S., Sheremet, M. A., Ganji, D. D., & Pop, I. Free convection of copper–water nanofluid in a porous gap between hot rectangular cylinder and cold circular cylinder under the effect of inclined magnetic field. *Journal of Thermal Analysis and Calorimetry*. 135(2): 1171-1184, 2019.
- [23] Shi, X., Jaryani, P., Amiri, A., Rahimi, A., & Malekshah, E. H. Heat transfer and nanofluid flow of free convection in a quarter cylinder channel considering nanoparticle shape effect. *Powder technology*. 346: 160- 170, 2019.
- [24] Hayat, T., Rashid, M., Alsaedi, A., & Asghar, S. Nonlinear convective flow of Maxwell nanofluid past a stretching cylinder with thermal radiation and chemical reaction. *Journal of the Brazilian Society of Mechanical Sciences and Engineering*. 41(2): 86, 2019.

Received Date: 29 Dec, 2018

Revised Date: 5 July, 2019

Published Date: 12 November 2019